photonics

MDPI

Review

Near-Field Laser Materials Processing: From Fundamentals to Emerging Trends in High-Resolution Nanomanufacturing

Iulia Anghel [1], Laura Ionel [1], Marian Zamfirescu [2] and Florin Jipa [2,*]

[1] National Institute for Laser, Plasma and Radiation Physics (INFLPR), Laser Department, Magurele, 077125 Bucharest, Romania
[2] National Institute for Laser, Plasma and Radiation Physics (INFLPR), Center for Advanced Laser Technology (CETAL), Magurele, 077125 Bucharest, Romania
* Correspondence: florin.jipa@inflpr.ro

Abstract

The fabrication of nanoscale structures beyond the diffraction limit of conventional optical systems remains a key challenge in modern photonics and laser materials processing. Near-field laser processing has emerged as a promising approach that relies on localized electromagnetic field enhancement in the vicinity of micro- and nanoscale structures. Unlike conventional optical systems, near-field techniques enable laser energy to be concentrated within deeply subwavelength regions, providing enhanced control over light–matter interactions and enabling the fabrication of structures at the nanoscale. Furthermore, the use of ultrafast femtosecond laser pulses enables precise energy deposition and localized material modification, offering opportunities to limit thermal effects. This review examines the fundamental mechanisms governing near-field enhancement, with particular emphasis on light scattering, dielectric field enhancement, photonic nanojet formation, and the role of particle geometry and optical properties. It discusses laser processing approaches based on dielectric colloidal particles, optically trapped microspheres, engineered optical masks, and the influence of liquid environments, highlighting their capabilities, limitations, and potential for parallel nanofabrication. Finally, recent advances and remaining challenges in process control, reproducibility, and scalability are discussed, outlining future directions for high-resolution and efficient laser-based nanomanufacturing.

Keywords: near-field; colloidal particles; microspheres; nano-processing; photonic jets; field enhancement; laser processing; Mie theory

1. Introduction

Laser-based technologies have become indispensable tools in modern materials processing owing to their exceptional versatility, high precision, non-contact operation, and ability to produce features with submicrometer resolution. The possibility of delivering electromagnetic energy to a well-defined region of a material, while accurately controlling parameters such as wavelength, pulse duration, repetition rate, fluence, irradiation dose, polarization, and irradiation environment, provides laser processing with a degree of flexibility that is difficult to achieve using conventional mechanical, chemical, or lithographic techniques. In addition, the absence of direct mechanical contact reduces tool wear, contamination, and mechanical loading of the workpiece, making laser-based methods particularly attractive for processing delicate structures and materials with complex geometries. Depending on the irradiation conditions and material properties, laser–matter

Check for updates

Received: 21 October 2026
Revised: 16 November 2026
Accepted: 23 November 2026
Published: 26 November 2026

Copyright: © 2026 by the authors. Licensee MDPI, Basel, Switzerland. This article is an open access article distributed under the terms and conditions of the Creative Commons Attribution (CC BY) license.

interactions can induce a broad range of effects, including heating, melting, vaporization, ablation, photochemical modification, phase transformation, surface restructuring, and changes in optical or electrical properties. Consequently, laser processing has found extensive application in fields such as microelectronics [1], photonics [2], biomedical engineering [3], energy technologies [4], surface functionalization [5], sensing [6], and micro- and nanofabrication [7]. The continuous miniaturization of functional devices, however, has imposed increasingly stringent requirements on the spatial resolution of laser-based fabrication. Modern photonic, electronic, biomedical, and sensing technologies frequently require structures with characteristic dimensions ranging from a few hundred nanometers down to several tens of nanometers. Achieving such dimensions by conventional laser processing remains challenging because the size of the irradiated region is fundamentally constrained by the diffraction of light. According to classical diffraction theory, electromagnetic radiation cannot be focused into an arbitrarily small volume. The lateral dimension of the focal spot is determined primarily by the irradiation wavelength and the numerical aperture of the focusing system and is typically on the order of approximately one-half of the wavelength [8]. Therefore, even when high-numerical-aperture optics are employed, conventional direct laser writing cannot readily provide the spatial confinement required for many emerging nanoscale applications.

Several strategies have been developed to reduce the effective processing dimensions beyond those predicted solely from the diffraction-limited focal spot. Two-photon lithography (TPL), also referred to as two-photon polymerization (2PP), represents an important approach to additive high-resolution laser-based micro- and nanofabrication where the enhancement effect is used. This process confines photopolymerization to a small three-dimensional volume (voxel), enabling the fabrication of complex structures with sub-diffraction-limited feature dimensions down to 30 nm [9] in the volume of photoresist materials. The achievable resolution and structural fidelity depend on several factors, including laser intensity, pulse duration, numerical aperture, exposure conditions, photoinitiator concentration, and the chemical properties of the photoresist [10–18]. Although TPP is generally based on nonlinear far-field focusing rather than near-field electromagnetic enhancement, it is relevant to the broader development of high-resolution laser nanofabrication. In contrast, near-field approaches exploit localized electromagnetic-field enhancement to confine energy deposition and induce material modification or removal at the nanoscale. Within this context, considerable attention has been directed toward approaches that manipulate the electromagnetic field directly in the proximity of micro- and nanoscale structures. In particular, near-field-enhanced laser processing has emerged as a powerful route for achieving highly localized energy deposition and, consequently, material modification at dimensions substantially below the conventional diffraction limit [19].

The fundamental distinction between conventional laser processing and near-field laser processing lies in the spatial characteristics of the electromagnetic field interacting with the material. In conventional laser processing, the irradiation field propagates through free space and is focused onto the sample using optical components such as lenses or microscope objectives. The minimum dimensions of the focal region are therefore governed by the diffraction limit. In contrast, when electromagnetic radiation interacts with an object having characteristic dimensions comparable to or smaller than the incident wavelength, strongly localized electromagnetic fields can develop in the immediate vicinity of the object. These fields contain spatial components that are not accessible through conventional propagating-wave focusing and can therefore exhibit characteristic dimensions considerably smaller than the free-space wavelength.

A variety of micro- and nanostructures can act as optical field concentrators. Representative examples include dielectric microspheres and nanoparticles, metallic nanoparticles

and nanostructures, structured substrates, nanoantennas, and sharp probes such as those employed in atomic force microscopy (AFM) and related scanning-probe techniques [20–22]. Depending on their geometry, dimensions, refractive index, dielectric properties, and interaction with the incident radiation, these structures can redistribute and concentrate electromagnetic energy within extremely small volumes. Dielectric particles, for example, can generate strongly confined photonic nanojets on their shadow-side surface [19], whereas metallic nanostructures may support localized surface plasmon resonances capable of producing substantial electromagnetic-field enhancement. Similarly, sharp metallic or dielectric tips can confine the optical field, enabling highly localized interactions between the enhanced electromagnetic field and the underlying material.

The physical mechanisms responsible for near-field enhancement are inherently linked to the interaction of electromagnetic radiation with structures whose characteristic dimensions are comparable to the wavelength of the incident light. When a laser beam interacts with such a structure, several optical phenomena including reflection, refraction, diffraction, absorption, and scattering may occur simultaneously. The incident and scattered electromagnetic waves interfere with one another, resulting in a complex spatial redistribution of the electric and magnetic fields. Under suitable conditions, constructive interference and resonant electromagnetic effects produce localized regions in which the field amplitude and optical intensity can significantly exceed those of the incident radiation. Because these fields are confined to the immediate vicinity of the micro- or nanostructure, they are generally referred to as optical near-fields. The characteristics of these localized fields depend strongly on both the optical properties and geometry of the field-enhancing structure. The optical response is therefore governed by a complex interplay between the electromagnetic properties of the enhancing structure, the irradiation conditions, and the optical and thermophysical properties of the processed material. Understanding these relationships is essential for transforming near-field enhancement from an interesting optical phenomenon into a reproducible and controllable nanofabrication strategy.

The present review aims to provide a broader perspective on the evolution of near-field laser materials processing, from colloidal particle-assisted techniques which predominantly rely on self-assembled dielectric microspheres for the fabrication of periodic nanoscale patterns to advanced methods for the fabrication of nanostructures with arbitrary geometries.

The review is structured as follows. Section 2 presents the electromagnetic principles underlying near-field enhancement and the numerical approaches for simulating electromagnetic wave propagation. Section 3 examines the main near-field laser processing configurations and their applications in micro- and nanofabrication. Section 4 provides a comprehensive discussion of the factors governing near-field enhancement and its relationship with material modification, addressing the influence of optical configurations, laser and material parameters, liquid environments, and different patterning strategies. Section 5 focuses on future directions regarding specific mechanisms and developments in near-field laser processing, including optical far-field-induced near-field breakdown and nanostructure growth driven by near-field enhancement for high-aspect-ratio nanostructures.

2. Analytical and Numerical Propagation Models

2.1. Theoretical Considerations

The physical mechanisms responsible for optical field enhancement have attracted significant scientific interest over the past several decades. Both theoretical and experimental investigations have contributed to a deeper understanding of light scattering by particles of various geometries, sizes, and optical properties.

Maxwell's equations provide the fundamental framework for describing electromagnetic fields and their interaction with matter. Within this framework, analytical and numeri-

cal approaches are used to determine the electromagnetic-field distributions associated with specific optical configurations. One of the most important analytical solutions describing electromagnetic scattering is Mie theory [23], which provides the exact solution for the interaction between a plane electromagnetic wave and a homogeneous spherical particle.

Mie theory represents a significant extension of the earlier Rayleigh scattering model. While Rayleigh's theory accurately describes scattering by non-absorbing dielectric particles much smaller than the wavelength of the incident radiation, typically with diameters far below the wavelength, its applicability rapidly decreases as particle dimensions become comparable to the wavelength. Mie's solution removed this limitation by providing a rigorous analytical description valid for spherical particles of arbitrary size, refractive index, and absorption characteristics. The theory predicts not only the total scattering intensity but also the angular distribution of scattered light, the internal electromagnetic field within the particle, and the highly localized field enhancement occurring in its immediate vicinity [24,25]. Mie resonances are also relevant to contemporary photonics, as they can be exploited to manipulate electromagnetic fields and control light–matter interactions [26] while a generalized Lorenz–Mie theory [27] was used to demonstrate the generation of photonic nanojets outside high-refractive-index microspheres using Gaussian-beam illumination [28]. Mie scattering exhibits several distinctive characteristics that are particularly relevant for near-field laser processing. First, the scattering pattern becomes strongly asymmetric, with most of the scattered energy concentrated in the forward propagation direction. Second, as the particle diameter increases, the scattered electromagnetic field becomes progressively more intense and spatially localized. These characteristics are responsible for the formation of nanophotonic jets and other localized electromagnetic phenomena that have attracted considerable attention for applications requiring sub-diffraction optical focusing. The original formulation of Mie theory assumes that the spherical particle is embedded in a non-absorbing surrounding medium. However, many practical laser-processing applications involve absorbing materials, where the optical response differs significantly from the ideal case. To overcome this limitation, several extensions of Mie theory have been proposed. Among the most notable are the models developed by Mundy [29] and by Bohren and Gilra [30], which extend the original analytical formulation to account for electromagnetic scattering in absorbing media. These theoretical developments have substantially broadened the applicability of Mie theory to realistic experimental conditions encountered in laser processing. A comprehensive treatment of electromagnetic scattering by particles of different sizes, shapes, and optical properties is provided by K.N. Liou [31]. His work presents both the theoretical foundations of scattering phenomena and numerous particular cases that have become reference solutions for subsequent analytical and numerical studies. Together with Mie's original formulation and its later extensions, these theoretical models constitute the basis for understanding optical near-field enhancement and light localization around dielectric particles. Lecler et al. show that the spatial characteristics of photonic nanojets, particularly the position of maximum irradiance and the lateral confinement of the optical field, are strongly influenced by the microsphere radius, refractive index, and illumination wavelength [32]. Since conventional geometrical optics cannot fully describe the electromagnetic interactions responsible for nanojet formation, rigorous approaches such as Lorenz–Mie theory are required to accurately predict their optical properties. Figure 1 illustrates the dependence of the axial position of the photonic nanojet intensity maximum on the microsphere refractive index (n_m) for different particle radii (r_0). The distance OP between the microsphere center O and the intensity maximum P, together with the particle radius, is normalized to the incident wavelength λ_0. For a fixed radius, increasing the refractive index shifts the intensity maximum toward the microsphere center, whereas increasing the radius at a constant refractive index moves the intensity

maximum farther from the center. The black markers indicate the transition at which the intensity maximum coincides with the microsphere surface (OP = r_0). The asymptotic behavior, represented by the dashed curve, suggests that for refractive indices exceeding approximately 1.83, the intensity maximum remains inside the microsphere, independently of its radius. This threshold differs from the value of approximately 2.0 predicted by geometrical optics in the large-particle limit, highlighting the importance of electromagnetic modeling. These findings demonstrate how microsphere geometry and refractive index can be tailored to control the spatial localization of photonic nanojets, providing valuable guidance for near-field optical applications and super-resolution imaging.

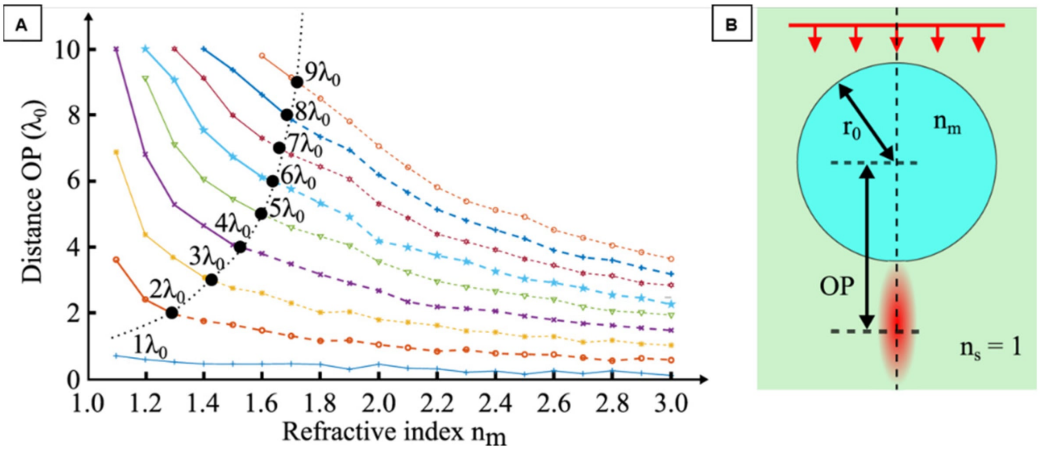


Figure 1. Axial position of the photonic jet irradiance maximum as a function of microsphere optical and geometrical properties. (**A**) Dependence of the photonic nanojet peak position (P) on the microsphere refractive index (n_m) for nine different radii (r_0), ranging from $1\lambda_0$ to $9\lambda_0$ in increments of λ_0. (**B**) Schematic representation of the Lorenz–Mie model, considering a dielectric microsphere illuminated by a plane wave of wavelength λ_0 in air ($n_s = 1.0$). The axial distance OP and microsphere radius r_0 are normalized to λ_0. Black dots indicate conditions where the irradiance maximum coincides with the microsphere surface (OP = r_0), separating external and internal focusing regimes (reprinted with permission from [32]).

2.2. Numerical Approaches for Simulation of Electromagnetic Wave Propagation

Software packages used for numerical simulation of optical field propagation, light confinement, dispersion, scattering, diffraction, and electromagnetic field enhancement are available both as commercial or open-source resources. All software are based on two distinct numerical implementations of Maxwell's equations solvers: Finite-Difference Time-Domain (FDTD) or Finite Element Method (FEM). These are dedicated numerical methods that allow investigation of local enhancement of electromagnetic fields in the vicinity of the photonic micro- and nanostructures. Both are suitable for investigation of near-field effects of nanophotonic structures. However, the methods present significant differences in terms of numerical software implementation, geometrical flexibility, computational costs and accuracy. The main software implementation difference between FDTD and FEM is related to time-domain and frequency-domain numerical solving of Maxwell's equations, Table 1. The FDTD is a time-domain method, employing a rectangular Yee-type spatial grid [33] and the successive updating of electric and magnetic field components. The fundamental principle of the FDTD method is based on the discretization of Maxwell's curl equations in both space and time. Using the FDTD method, the optical field components are calculated iteratively at each time step as both fields propagate through complex structures. The electric and magnetic field components are positioned at different locations to achieve numerical stability and accurately represent electromagnetic wave propagation.

The algorithm is relatively simple to implement and efficient to parallelize, including on GPU architectures. Software packages such as RSoft [34–40], Ansys Lumerical FDTD [41], MEEP [42,43], OmniSim FDTD [44], and CST Studio Suite provide advanced tools for electromagnetic simulations based on FDTD. In contrast, FEM utilizes the discretization of the domain into finite elements and typically solves Maxwell's equations in the frequency domain through large-scale systems of algebraic equations. Its implementation is mathematically and computationally more complex, requiring the generation of a discretization grid (mesh), variational formulations, and specialized solvers. Platforms such as COMSOL Multiphysics [45,46], and the open-source libraries NGSolve/Netgen offer a high degree of flexibility for developing custom electromagnetic models.

When choosing one or other numerical tool, several advantages versus limitations are considered. Flexibility of choosing a particular geometry is one of the first criteria. FDTD is using a Cartesian grid, a clear and straight forward step to implement, that comes with serious limitations in approximating curved surfaces and inclined edges, especially on subwavelength geometries. Higher spatial resolution, respectively finer temporal grid, is usually necessary in order to avoid any numerical artifacts because of pixelization. A subsequent refinement of pixel discretization and convergence study is required in order to obtain better results. However, that comes with an additional computational cost. FEM offers a significant advantage by employing tetrahedral or triangular elements, that are adapted to the desired geometry, including curved elements. This feature facilitates the simulation of microcones, microlenses, aspheric structures, nanotips, and three-dimensional architectures fabricated via 3D laser lithography or Two-Photon Polymerization (TPP).

Computational cost is one of the criteria that filters the final decision of choosing the most appropriate numerical methods. In FDTD, reducing the spatial step size leads to a rapid increase in the number of cells and necessitates a reduction in the time step to satisfy the Courant–Friedrichs–Lewy (CFL) stability condition. In three-dimensional simulations, halving the spatial step size can increase the computational cost by approximately a factor of 16 for the same simulated physical duration. FEM allows for local refinement of the discretization in regions of interest, thereby reducing the number of degrees of freedom required to describe fine geometric details. However, solving sparse matrix systems can demand significant memory and processing resources. FDTD is particularly efficient for broad-spectrum analysis, as a single simulation with broadband excitation can provide the response at multiple frequencies, whereas FEM generally requires successive solutions for each frequency being analyzed.

Both methods can be used for simulation of near-field optical enhancement, once the chosen method is adapted to a specific geometry. FDTD is advantageous for investigating the temporal evolution of the field, the propagation of ultrafast laser pulses, and the spectral response of resonant structures. FEM is particularly well-suited for determining local field distributions in the vicinity of curved surfaces, tips, and regions with high electromagnetic gradients. Adaptive refinement enables the precise characterization of the position, size, and amplitude of enhancement regions, the so-called hotspots, provided that numerical convergence is verified and physically realistic geometries are used.

For the investigation of near-field optical enhancement produced by complex dielectric microstructures and nanostructures, FEM is generally the preferred choice when the primary objective is geometric optimization and the determination of the spatial field distribution at selected wavelengths. The FDTD method offers complementary advantages for broadband analysis and the simulation of the electromagnetic dynamics of laser pulses. Combining these two methods can ensure both the efficient optimization of structures and the independent validation of numerical results.

FDTD and FEM share several important capabilities for near-field electromagnetic analysis. Both can describe the interaction of incident electromagnetic radiation with dielectric micro-objects and predict the spatial redistribution of optical intensity resulting from diffraction, scattering, and interference. They also allow systematic investigation of the influence of wavelength, polarization, refractive index, particle dimensions, and geometrical configuration on localized electromagnetic field enhancement. Their principal differences arise from the numerical discretization and solution domains. FDTD generally uses structured spatial grids and time-domain calculations, making it particularly suitable for broadband electromagnetic analysis, whereas FEM commonly employs geometry-conforming meshes and frequency-domain formulations, offering flexibility for complex geometries and wavelength-specific investigations. The accuracy of both approaches depends on appropriate spatial discretization, material descriptions, boundary conditions, and numerical convergence.

Table 1. FDTD versus FEM comparison as numerical simulation tools of optical near-field enhancement.

Criteria	FDTD	FEM
Numerical implementation of Maxwell equations	Temporal domain. Computation of E and H components based on Yee-type spatial grid.	Frequency domain. Solver of wave vectorial equation.
Spatial discretization	Regular grid, requires incremental increase in spatial resolution.	Flexible mesh adapted to the geometry.
Computational cost	Exponential increase with reducing the spatial and temporal steps Good prediction of necessary RAM memory due to regular grid, Parallelization is possible.	Depends on structure complexity and matrix solver. RAM requirements strongly dependent on structure design. Parallelization is possible depending on solver architecture.
Spectral analysis	Broadband excitation allows for broad spectral analysis.	Requires separate computation of each frequency.
Ultrashort-pulse analysis	Direct computation of temporal evolution of the field.	Possible from spectral reconstruction.
Near-field hotspot analysis	Good accuracy depending on grid discretization and computational resources.	Good accuracy due to adaptive mesh. Complex structures require more memory.

It is important to mention that, in very high-intensity laser regimes, both linear electromagnetic approaches must be extended or coupled with additional models to account for ionization, plasma formation, and other nonlinear effects, that cannot be predicted in a linear regime as provided by FDTD and FEM simulation.

The achievable near-field enhancement effect is fundamentally constrained by the electromagnetic properties of the field-enhancing structure, the incident wavelength, material losses, and the spatial confinement of the generated field. Although theoretical models predict strong local-field intensification under optimized conditions, practical enhancement is limited by factors such as absorption, fabrication imperfections, particle–substrate interactions, and the stability of the optical configuration. These constraints are particularly relevant to dielectric microspheres and structured substrates, where particle dimensions, refractive index, geometry, and surrounding medium determine the intensity, spatial extent, and position of the enhanced field. Understanding these theoretical limitations provides an important basis for interpreting the practical performance of the near-field configurations presented in this review.

3. Experimental Approaches for Near-Field Laser Processing

Although theoretical models and numerical simulations provide valuable insights into the mechanisms governing electromagnetic field localization and enhancement, experimental investigations are essential for validating these predictions and establishing their practical applicability to laser-based micro- and nanofabrication. Processes such as localized heating, melting, ablation, material redistribution, and re-solidification can significantly influence the final morphology of laser-induced structures. Consequently, experimental studies play a fundamental role in correlating calculated electromagnetic field enhancement with the resulting material modifications and in identifying the conditions required for reproducible nanoscale processing.

The following section examines representative experimental approaches to near-field-enhanced laser processing, focusing on configurations employing dielectric colloidal particles and photoresist structures. Particular emphasis is placed on the influence of field-enhancing geometry, irradiation parameters, substrate properties, and processing environment on the achievable spatial resolution and resulting surface morphology. Experimental investigations performed in air and liquid environments are considered to illustrate how electromagnetic field localization can be translated into controlled material modification. By connecting theoretical predictions and numerical simulations with experimentally observed results, these studies provide a basis for evaluating the capabilities, limitations, and potential applications of near-field-enhanced laser processing in advanced micro- and nanofabrication.

3.1. Near-Field Laser Material Processing in Air

3.1.1. Self-Assembled Colloidal Lithography Technique

The colloidal lithography technique employs a self-assembly two-dimensional (2D) ordered arrays of colloidal particles with diameters ranging from several hundred nanometers to several tens of micrometers [47]. Upon laser irradiation, each microsphere acts as a microlens, concentrating the incident light into highly localized regions of maximum intensity underneath the particles [48–52].

Depending on the laser parameters and material properties, this can lead to localized modification of the material structure, or other permanent changes at the micro- and nanoscale. The spatial distribution of the resulting patterns is therefore strongly related to the local electromagnetic field distribution and fluence. Wet self-assembly is a simple, cost-effective, bottom-up technique for organizing colloidal micro- and nanoparticles into ordered structures through capillary forces, interparticle interactions, and solvent evaporation. Common deposition methods include drop-casting, spin-coating, dip-coating, and convective self-assembly, which can produce closely packed monolayers with hexagonal ordering or even a dry manual assembly on nanolithographically patterned substrates [53]. Employing such techniques, the self-arranged hexagonal configuration of particles can be changed into a square configuration, Figure 2, demonstrating the potential of this technique to generate variable configurations of microspheres. Silica (SiO_2) and polystyrene (PS) microspheres are frequently employed due to their uniform dimensions and suitable optical properties. In near-field laser ablation, self-assembled dielectric microspheres act as microlenses, concentrating incident laser radiation into highly localized intensity regions near the substrate surface through photonic nanojet formation. When the enhanced optical intensity exceeds the material ablation threshold, localized material removal occurs, enabling the fabrication of periodic micro- and nanostructures with feature sizes potentially smaller than the incident wavelength.

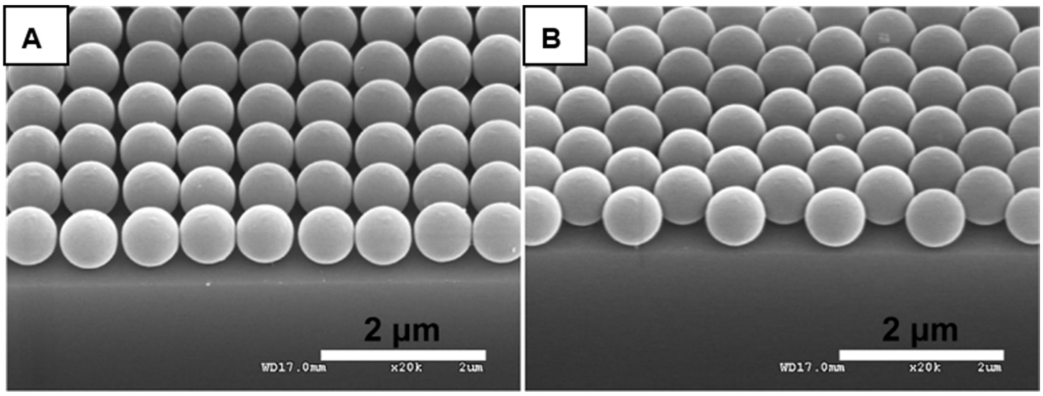


Figure 2. Scanning electron microscope (SEM) images of 700 nm sized silica microspheres organized in square (**A**) and hexagonal (**B**) patterns (reprinted with permission from [53]).

One of the main benefits of this method is the simplicity and low cost of the fabrication process, which eliminates the need for expensive lithographic masks or complex optical focusing systems. The spontaneous organization of colloidal microspheres into ordered arrays enables parallel fabrication of periodic micro- and nanostructures over relatively large surface areas, significantly improving processing efficiency compared with serial laser writing techniques. Another important advantage is the flexibility of the technique, since the dimensions and periodicity of the fabricated structures can be adjusted by selecting the microsphere diameter, refractive index, and laser irradiation parameters. Additionally, the method is compatible with various substrate materials, including metals, semiconductors, and polymers, provided that suitable laser–material interaction conditions are established.

Despite its advantages, self-assembly combined with near-field laser ablation presents several limitations concerning pattern flexibility, uniformity, and reproducibility. One major limitation is the self-organized arrangement of colloidal particles, which generally produces periodic, closely packed patterns and restricts the fabrication of arbitrary or independently positioned micro- and nanostructures, although nonhexagonal patterns can be created by focusing a laser on each particle [54]. Moreover, structural defects, particle aggregation, and incomplete monolayer coverage can introduce irregularities in the resulting ablation patterns. Another important limitation arises from the Gaussian spatial energy distribution of conventional laser beams, which produces nonuniform irradiation across the assembled microsphere array. Consequently, particles located near the beam center experience higher incident fluence than those at the periphery, leading to variations in ablation depth, feature diameter, and, in some cases, incomplete material removal. Additionally, the near-field enhancement strongly depends on microsphere diameter, refractive index, particle–substrate separation, and laser wavelength, making the process sensitive to geometrical and experimental variations. Particle displacement or damage during laser irradiation, together with difficulties in controlling the local energy deposition, can further reduce pattern reproducibility. These limitations constrain the fabrication of large-area, homogeneous, and precisely controlled nanostructures, highlighting the need for improved particle positioning and laser beam homogenization strategies. However, the dry manual assembly method proposed by Khanh and Yoon (2009) [53] offers new perspectives, particularly improved control over colloidal particle positioning and arrangement. By combining mechanically driven particle assembly with pre-patterned substrates, this approach enables the fabrication of highly ordered one- and two-dimensional particle arrays with reduced structural defects and improved reproducibility. Furthermore, the absence of solvent evaporation minimizes drying-related defects, such as particle aggregation and coffee-ring formation. This method is particularly promising for microsphere-assisted near-field laser ablation,

where precise particle positioning and uniform spacing are essential for obtaining controlled and reproducible surface patterns.

3.1.2. Near-Field Laser Processing Based on Trapped Microsphere

Array-based optical nanolithography provides an effective approach for producing multiple nanoscale features simultaneously over a relatively large area. The method relies on the use of microspheres as near-field optical probes, which locally concentrate the incident laser radiation and enable the formation of features below the diffraction limit. However, this method provides structures that are arranged in hexagonal or squared patterns, but offers limited control over the positions of individual microspheres. Different patterns and new feature dimensions can be obtained by changing the microsphere position using trapped microspheres. A similar concept was proposed by Yin et al. [55], fixing the microsphere to a holder, Figure 3A. Microsphere-assisted laser nano-structuring provides a method for producing nanoscale surface features as small as approximately 38 nm ($\lambda/27$) by locally concentrating the incident laser radiation. In this approach, the microsphere modifies the spatial distribution of the incident beam and produces a tightly confined photonic nanojet near the substrate surface. The resulting localized energy distribution can be used to control the dimensions of the structures produced on the material. An important advantage of this configuration is that nanoscale features can be obtained under far-field irradiation and in ambient air, without requiring a near-field probe or a conventional nanolithography system. The principle and experimental implementation of this approach are illustrated in Figure 3, in which a microsphere is positioned above the Sb_2S_3 thin film and used to focus the incident laser radiation. The authors use a microsphere with a diameter of approximately 50 µm, producing a photonic nanojet with a FWHM of about 920 nm. Figure 3B,C show the resulting nano-lines obtained for different laser polarization directions. The AFM image and line profile demonstrate that the structures remain similar when the polarization angle is varied from 0° to 90°. The corresponding profiles in Figure 3D confirm this behavior, with the measured groove widths remaining approximately between 50 and 60 nm. This demonstrates that the proposed process can produce nanoscale structures with reduced dependence on the polarization direction.

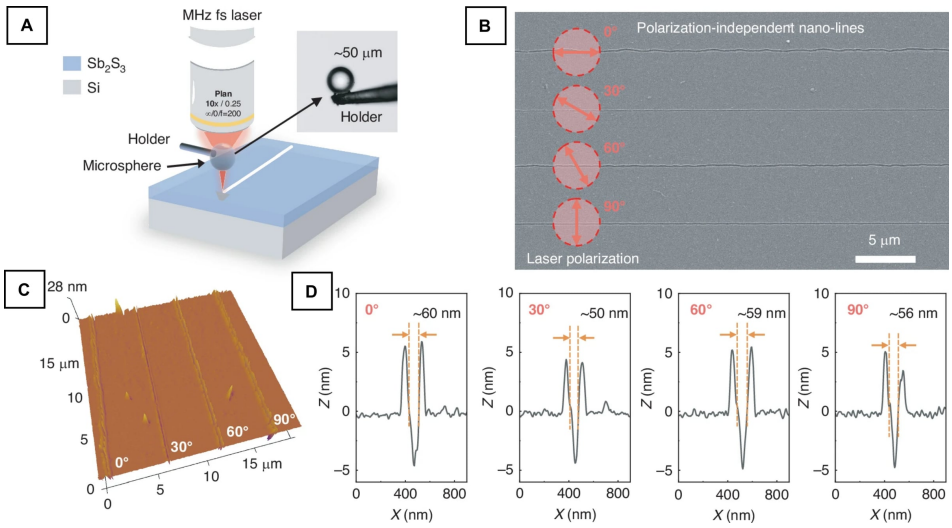


Figure 3. Demonstration of optical nanolithography using optically trapped microspheres: (**A**) experimental configuration for laser irradiation through trapped microsphere, (**B**) Optical image of the fabricated nano-lines, (**C**) AFM morphology of the processed surface, and (**D**) corresponding cross-sectional profiles obtained for different laser polarization angles (reprinted with permission from [55]).

The difference between the photonic nanojet width (FWHM ≈ 920 nm) and the resulting groove dimensions (approximately 50–60 nm) can be attributed to the threshold-dependent nature of laser-induced material modification. Although the enhanced optical field extends over a relatively broad region, material removal occurs only where the local laser intensity exceeds the ablation threshold. Furthermore, nonlinear laser–matter interactions can contribute to confining material modification to a region substantially narrower than the optical intensity distribution. Consequently, the final feature dimensions are not determined solely by the spatial width of the photonic nanojet, but also by the local intensity distribution and the material response under the applied irradiation conditions.

3.1.3. Near-Field Laser Processing Based on Polymer Structures

An alternative approach to conventional colloidal microsphere-assisted near-field laser ablation is to employ lithographically patterned photoresist masks to control the spatial distribution of electromagnetic energy during femtosecond laser irradiation. The proposed method introduced by Jipa et al. addresses several limitations associated with self-assembled colloidal particles, particularly the restricted flexibility of periodic patterns, difficulties in controlling particle positioning, and sensitivity to the particle–substrate separation [56]. Unlike conventional microsphere-based approaches, where localized optical enhancement is generated by individual dielectric particles, the authors employed engineered polymethyl methacrylate (PMMA) microstructures to produce controlled near-field intensity distributions over extended regions [56,57]. The experimental results presented in Figure 4A–F demonstrated the parallel fabrication of continuous nanoscale grooves on silicon substrates using a single infrared femtosecond laser pulse at 775 nm wavelength. By employing a photoresist mask with a periodicity of 2 μm Figure 4A, a feature width of 1 μm, Figure 4D, and a thickness of approximately 300 nm, the authors obtained grooves with widths of approximately 250 nm, Figure 4C,F, significantly smaller than both the irradiation wavelength and the characteristic dimensions of the mask structures. An additional advantage of the proposed technique is the possibility of reusing the transparent photoresist mask, owing to its higher laser damage threshold relative to the silicon substrate under the investigated irradiation conditions. Furthermore, lithographic fabrication enables greater control over mask geometry and spatial arrangement, potentially allowing more complex surface patterns than those achievable through spontaneous colloidal self-assembly.

This work demonstrated the feasibility of single-pulse, parallel laser nanofabrication using engineered dielectric masks, combining subwavelength resolution, controlled optical field enhancement, and improved geometrical flexibility. These findings highlight the potential of photoresist-assisted near-field laser processing as a promising strategy for high-throughput surface nanopatterning, although large-area uniformity and scalability require further investigation. The use of photoresist masks in near-field femtosecond laser ablation provides a practical approach for parallel nanofabrication.

A similar approach, targeting the fabrication of arbitrary patterns was introduced by Khudiyev et al. where the optical field is concentrated into a region smaller than the dimensions of the structure, allowing the incident radiation to be transferred locally to a photosensitive material [58]. Such a configuration can provide mask-free patterning and can be used to generate one-dimensional nanoscale structures with controlled geometry. The method introduced photonic nanoblade lithography based on the forward-scattering and focusing properties of low-refractive-index polymer nanowires, demonstrating their potential for direct nanoscale patterning. Figure 4G,H shows the experimental configuration used for the proof-of-concept demonstration, where a single core–shell polymer nanowire is positioned on a photoresist-coated substrate. During UV irradiation, the nanowire acts as an optical element that concentrates the scattered light onto the photoresist. After exposure

and development, the localized illumination produces a pattern corresponding to the optical path defined by the nanowire. As shown in Figure 4H, the resulting structure reproduces the shape of the nanowire, demonstrating that the near-field focusing effect can be used to create nonlinear and non-periodic nanoscale patterns without a conventional photomask. The authors report a nanohole width of approximately 400 nm for a polymer wire with a thickness of 3.2 µm.

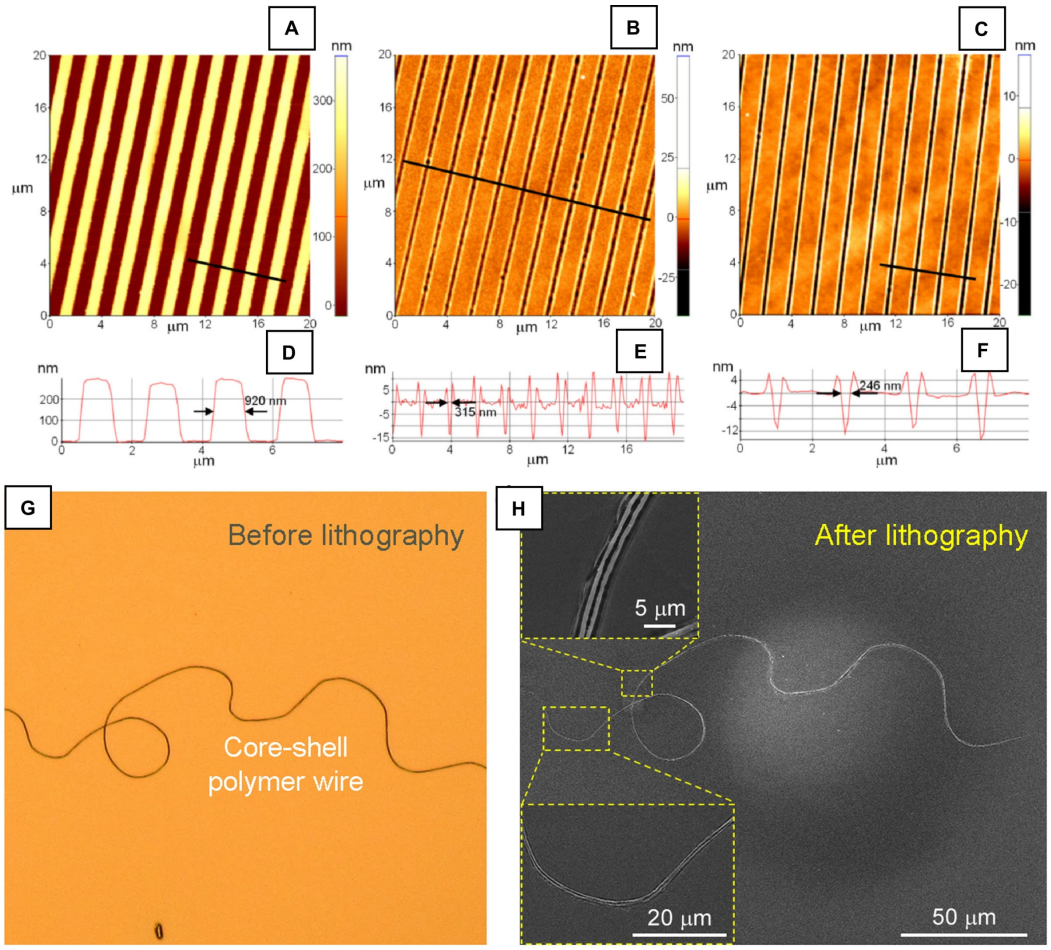


Figure 4. Patterns created by near-field enhancement. (**A**) AFM images of the fabricated optical mask with its profile (**D**) and corresponding imprinted surface profiles illustrating the transfer of the photoresist mask pattern onto the silicon substrate (**B**,**C**) with profile (**E**,**F**), through single-pulse femtosecond near-field laser ablation (reprinted with permission from [56]); (**G**) polymer nanowire positioned on a photoresist-coated substrate during UV exposure and (**H**) resulting one-dimensional nanopattern after photoresist development, reproducing the path of the nanowire (reprinted with permission from [58]).

3.2. Near-Field Laser Material Processing in Liquids

3.2.1. Influence of the Surrounding Refractive Index on Light Propagation and Field Localization

Laser materials processing in a liquid environment became an attractive field for scientists, engineers and manufacturers due to the markedly different propagation and enhancement of electromagnetic fields in the near-field regime [59–62]. The presence of the liquid significantly modifies the laser–material interaction and can improve the quality and efficiency of processes such as surface modification [63], drilling [64], cleaning [65], nanoparticle production [66], and microfabrication [67].

The main scientific interest lies in understanding the fundamental mechanisms governing the interaction between intense laser pulses and materials exposed to either chemically reactive or non-reactive environments. From an engineering and manufacturing perspective, lasers represent a powerful tool capable of making the production process more economical, faster, cleaner, and more precise. The concept of laser materials processing in a liquid environment using nano- and microspheres is relatively simple and employs a predefined surface with self-assembled two-dimensional (2D) ordered arrays of colloidal particles, which is immersed in different types of liquid precursors. The liquid precursors are chosen depending on the etching activity they can induce on the surfaces (on which the microspheres are deposited) due to the laser excitation of the molecules contained in the liquid precursors. Also, the microsphere size, refractive index, concentration and material are some of the most important parameters because they determine how strongly the microspheres interact with the laser beam. The liquid environment plays several important roles in the laser processing process such as reducing the thermal effect, limiting the heat-affected zone and removing the surplus material accumulated in the laser processing area or even changing the refractive index of the particle surrounding medium. Short- and ultrashort-pulse lasers are very attractive for this kind of experiment because they deliver a significant amount of energy in a short time, limiting heat diffusion and enabling precise material removal. The combination of laser energy, particle-assisted optical effects, the cooling and transport properties of liquids provides additional control over material modification [68].

The behavior of an electromagnetic field in air and water was demonstrated by Wang et al. [69], showing that the focal position of the enhanced optical field can be adjusted by modifying the optical environment surrounding the particles. The spatial distribution and focusing characteristics of photonic nanojets can be effectively controlled by adjusting the incident laser focal position and wavelength. As illustrated in Figure 5, Rahman et al. investigated these effects using three-dimensional finite-difference time-domain (3D-FDTD) simulations of an 8 μm silica microsphere immersed in water, considering the fundamental laser wavelength (1030 nm) and its second harmonic (515 nm) [70]. The results demonstrate that the formation and axial localization of the photonic nanojets are strongly dependent on the laser defocusing distance, with external nanojet formation occurring at approximately −9 μm and −8 μm for the fundamental and second-harmonic wavelengths, respectively. Increasing the defocusing distance progressively shifts the photonic nanojet intensity maximum away from the microsphere surface, extending its working distance and depth of focus, while producing relatively minor variations in the lateral beam diameter, Figure 5A–D. The shorter wavelength provides stronger lateral confinement, generating a narrower photonic nanojet compared with the fundamental wavelength. Under the selected focusing conditions, the 515 nm beam produces a lateral diameter of 0.43 μm and a working distance of 4.18 μm, compared with 0.73 μm and 2.84 μm at 1030 nm, respectively Figure 5E,F. However, the fundamental wavelength exhibits a slightly greater axial depth of focus (3.16 μm versus 2.51 μm). These findings highlight the potential of combining wavelength selection and incident beam focusing to independently influence the spatial confinement and axial localization of photonic nanojets, offering additional flexibility for high-resolution laser processing and near-field optical applications.

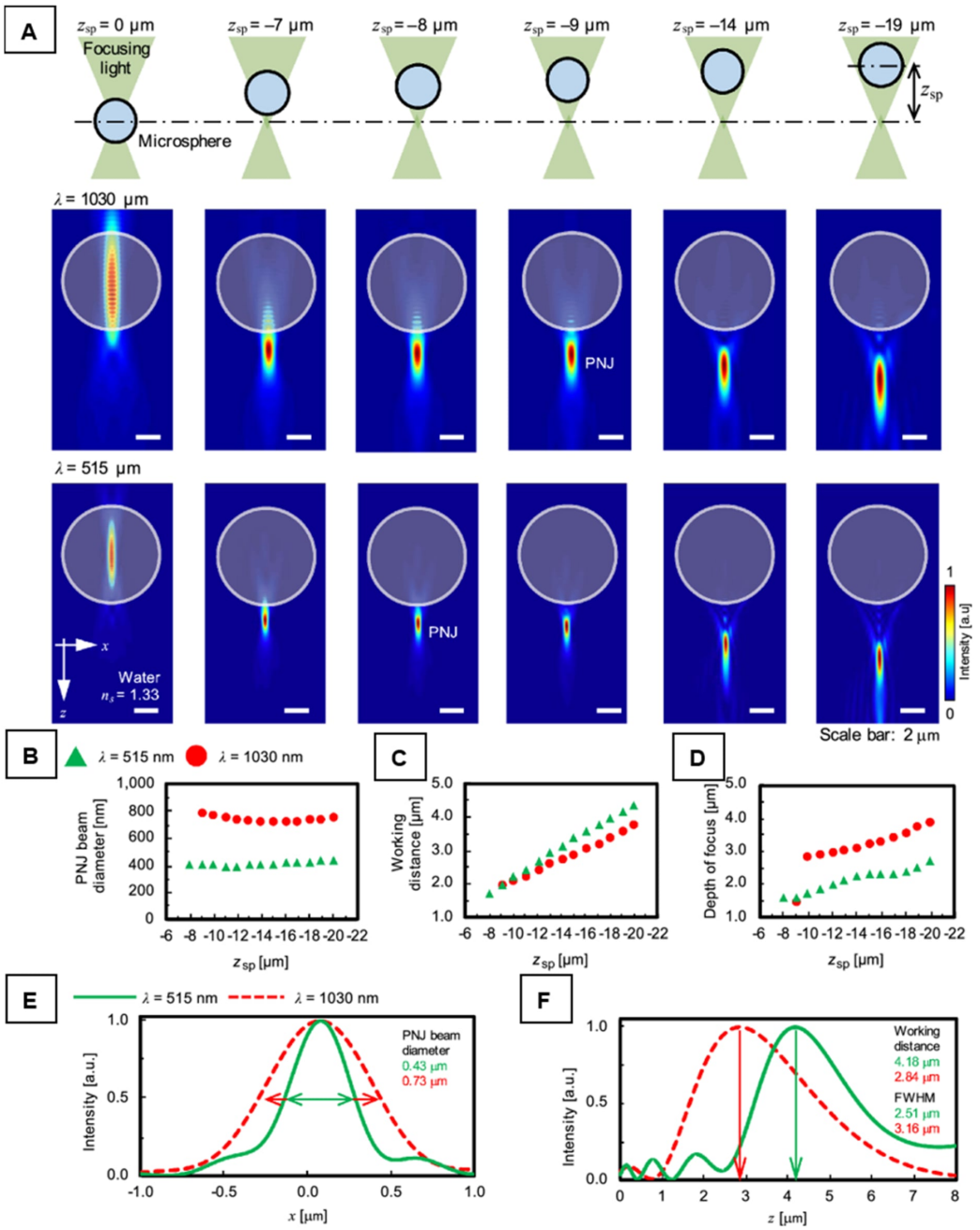


Figure 5. Influence of laser focal position on the photonic nanojet characteristics at the fundamental wavelength and its second harmonic generation (SHG). (**A**) Spatial intensity distribution of the photonic nanojets; (**B**) photonic nanojet beam diameter; (**C**) working distance; and (**D**) depth of focus as functions of the laser focal position. Experimentally obtained photonic nanojet intensity profiles along (**E**) the transverse (x) direction at the position of maximum intensity and (**F**) the axial (z) direction (reprinted with permission from [70]).

Similar work was performed by Ulmeanu et al. showing how the refractive index of the surrounding liquid influences the focusing behavior and near-field intensity generated by a silica colloidal particle [71]. The calculated Poynting vector distribution shown in Figure 6A illustrates the changes in the direction and spatial extent of the directional energy flux for different surrounding media. In air, Figure 6A shows that the focal region is located close to the particle surface, at approximately $Z/R = 1.2$, with the field enhancement decreasing rapidly along the propagation direction. When the particle is immersed in a liquid with $n_{\mathrm{liquid}} = 1.35$, as shown in Figure 6B, the focal position shifts further from the particle,

reaching approximately $Z/R = 4.2$, while the enhanced field remains concentrated along the optical axis over a longer distance. This behavior indicates that a surrounding medium with a refractive index lower than that of the silica particle can extend the focal region and potentially improve energy coupling into deeper regions of the substrate. In contrast, Figure 6C, corresponding to $n_{liquid} > n_{colloid}$, shows that the strongest field enhancement is concentrated near the edges of the particle rather than along the central optical axis. The comparison between these configurations demonstrates that the refractive index of the surrounding medium provides effective control over the position and spatial distribution of the near-field intensity, which is particularly relevant for localized laser processing and particle-assisted patterning. The SEM images from Figure 6D–F demonstrate the capability of this method to generate highly ordered two-dimensional patterns over extended areas using a monolayer of silica colloidal particles.

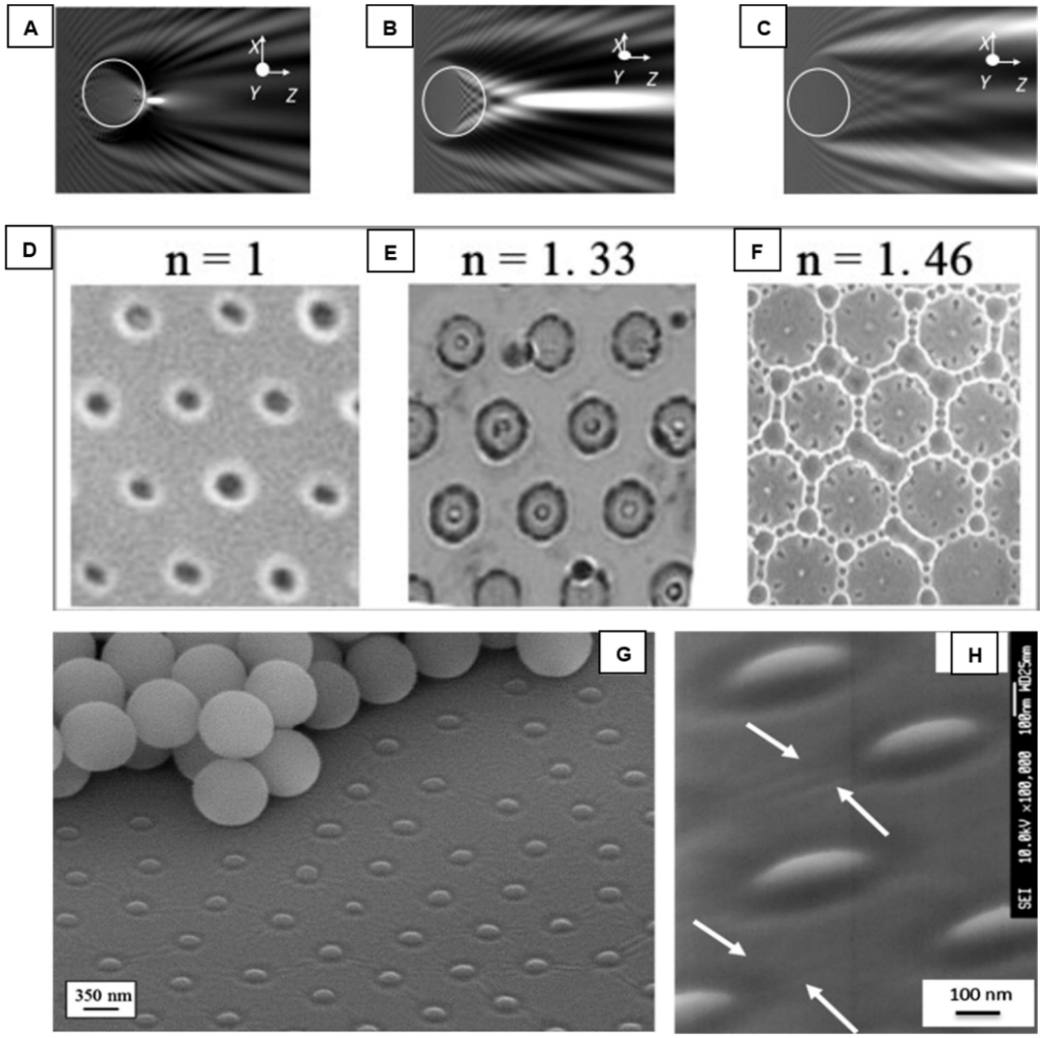


Figure 6. Near-field laser enhancement in different media. Calculated Poynting vector $|S_z|$ distributions around a single silica particle ($R = 1.5$ μm, $n_{colloid} = 1.44$) for surrounding media with refractive indices of (**A**) 1.00, (**B**) 1.35, and (**C**) 1.49. The simulations consider a linearly polarized beam ($\lambda = 400$ nm) incident along the Z-direction. SEM images showing the Si surface after single-shot laser processing in (**D**) air ($n = 1$), (**E**) CH_3OH ($n = 1.33$), (**F**) CCl_4 ($n = 1.46$). The pattern generated by a double layer of colloidal particles in CH_3OH ($n = 1.33$) is shown in (**G**) with the inset in (**H**) showing micro-cracks by arrows (reprinted with permission from [71]).

The extension of the effective focal length when using a liquid with a refractive index lower than that of the colloidal particles (n_liquid < n_colloid) enables near-field laser

patterning through multilayer colloidal arrays, Figure 6G,H. Ulmeanu et al. demonstrated this approach using a double layer of silica particles (R = 350 nm) immersed in methanol (CH_3OH). Figure 6F,G presents 60° tilted SEM images of a silicon surface irradiated with a single laser pulse, revealing periodic protrusions with base diameters of approximately 300 nm and heights of 100 nm. The formation of these structures demonstrates the feasibility of localized surface modification through multilayer particle assemblies. However, the surrounding regions of mild ablation and the presence of narrow cracks suggest that laser-induced thermal and mechanical stresses may affect surface quality. These results highlight the potential of liquid-assisted colloidal lithography for three-dimensional nanopatterning, while emphasizing the importance of controlling irradiation conditions to minimize undesirable surface damage.

3.2.2. Influence of Liquid Etching Media on Light Propagation and Near-Field Focusing

Other works were focused on the chemical precursors which influence the substrate chemistry during laser irradiation, completely changing the imprinted pattern [72]. Ulmeanu et al. present an efficient technique to produce periodic arrays of nanostructures on silicon and gallium arsenide substrates using near-field enhanced laser irradiation in the presence of liquid precursors, Figure 7 [48,49]. The study shows the limitations imposed by conventional far-field optical processing, particularly the diffraction limit, by exploiting the optical near-field generated around an ordered array of silica microspheres. The experimental procedure employs a self-assembled array of monodisperse silica colloidal particles with a diameter of approximately 700 nm on Si and GaAs substrates. The substrates were irradiated at normal incidence using a single 200 fs laser pulse at a wavelength of 387 nm. Importantly, the colloidal particle arrays were immersed in different liquid precursors, namely acetone ($n = 1.3644$), carbon tetrachloride ($n = 1.4625$), and 1,1,2-trichlorotrifluoroethane ($n = 1.43$). The liquids were selected not only because of their different refractive indices, quite close to the refractive index of the silica microspheres, but also because of the chemical activity of hydrogen-, chlorine-, and fluorine-containing species toward silicon. Consequently, the liquid environment plays an important role in modifying the optical near-field distribution as well as the photochemical and photothermal processes occurring during laser irradiation. Changing the surrounding liquid modifies the refractive-index contrast between the silica particles and their environment, thereby altering the position and characteristics of the enhanced optical field. This provides an additional means of controlling the morphology of the laser-induced structures. The experiments demonstrate that different types of periodic surface morphologies can be obtained, including ring-shaped bumps (width of about 230 nm, thickness of the wall of about 50 nm and a height of about 6 nm) Figure 7A, disk-like and convex bumps Figure 7C,D, as well as holes Figure 7B. The structures are arranged according to the regular two-dimensional, predominantly hexagonal, organization of the silica microspheres. The morphology depends strongly on the laser fluence, the number of colloidal layers, the substrate material, and the liquid surrounding the particles. It was demonstrated that the technique can effectively generate ordered nanostructure arrays on both silicon and gallium arsenide surfaces, materials widely used in microelectronics and optoelectronics. The periodic arrays exhibit uniform size distribution and spatial arrangement, which are crucial for applications in photonic devices, sensors, and nanoscale material studies. The surface morphology obtained during liquid-assisted near-field processing results from the combined contributions of electromagnetic, thermal, and chemical effects. Changes in the surrounding refractive index modify the scattering conditions and spatial distribution of the enhanced optical field, thereby influencing the location and extent of material modification. In parallel, laser-induced heating can promote melting, material redistribution, or localized ablation, depending on the deposited energy

and thermal properties of the substrate and liquid. When reactive liquid precursors are used, additional chemical processes may contribute to material removal, deposition, or surface functionalization. The relative importance of these mechanisms depends on the laser parameters, liquid composition, and substrate properties, ultimately determining the morphology, dimensions, and uniformity of the fabricated features.

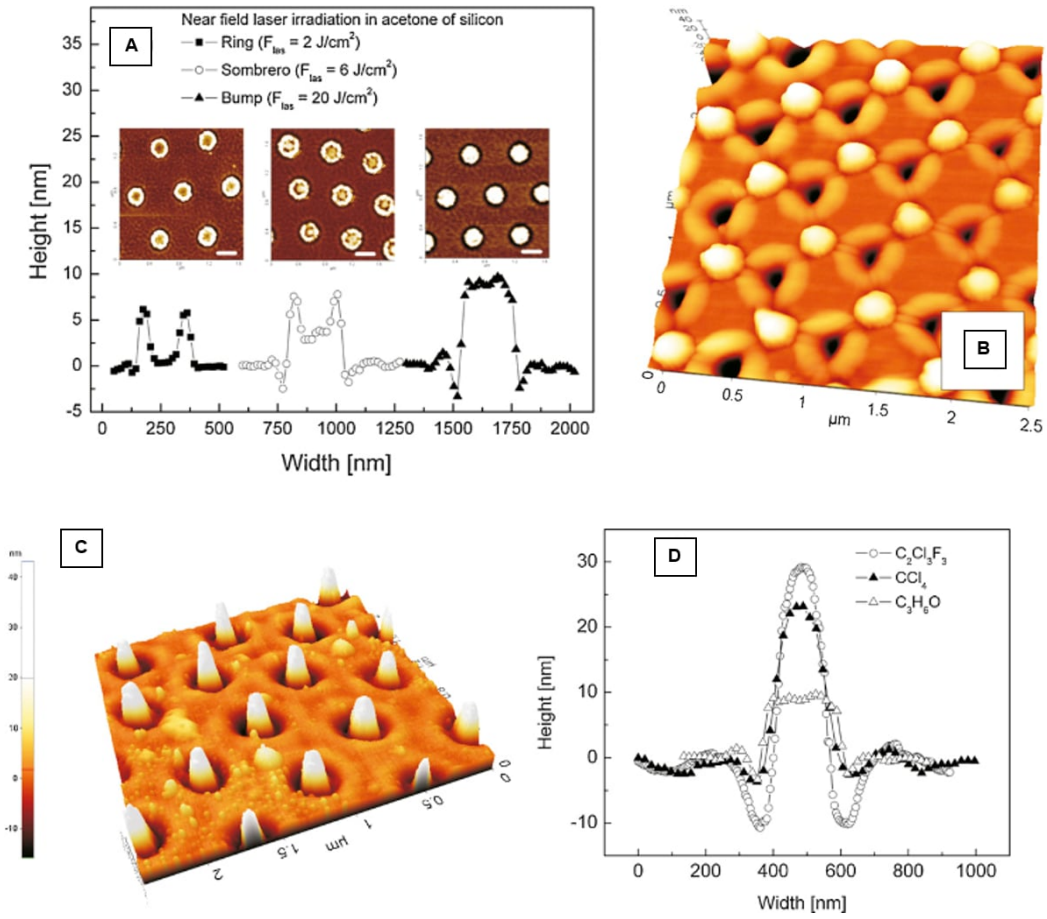


Figure 7. Atomic force microscopy (AFM) images of hexagonal array of (**A**) ring-bumps; sombrero-bumps and disk-bumps obtained on silicon surface immersed in acetone after a single femtosecond laser irradiation at different pulse energies through a self-assembled 700 nm silica particles monolayer array; (**B**) combination of holes and convex bumps generated on silicon surface immersed in tetrachloride; (**C**) convex Si bump immersed in trichlorotrifluoroethane; (**D**) profiles of each Si bump obtained with the three liquid precursors (reprinted with permission from [48,49]).

4. Discussion

The methods discussed in this review reflect a transition from periodic, particle-defined hole arrays towards deterministic and geometrically flexible surface nanopatterning. All these approaches differ in terms of achievable feature dimensions, processing flexibility, and practical implementation. Despite sharing the same underlying principle of localized electromagnetic-field enhancement, these techniques differ considerably in terms of achievable feature dimensions, pattern flexibility, processing throughput, reproducibility, and scalability. Consequently, their suitability for specific nanomanufacturing applications depends not only on their spatial resolution but also on the degree of control over particle positioning, optical configuration, irradiation conditions, and substrate properties.

Self-assembled colloidal lithography enables the parallel fabrication of periodic sub-wavelength structures over relatively large areas, offering high throughput but limited flexibility in pattern geometry and sensitivity to particle distribution and arrangement.

Depending on the particle dimensions, optical properties, laser parameters, and substrate response, these configurations can produce features ranging from hundreds of nanometers to several tens of nanometers. However, its reliance on spontaneous particle organization restricts the fabrication of non-periodic structures and patterns with arbitrary geometries. Moreover, vacancies, particle aggregation, and variations in particle size or interparticle spacing can introduce spatial variations in electromagnetic-field enhancement, consequently affecting feature dimensions and morphological uniformity.

An alternative strategy involves the use of engineered optical masks, particularly photoresist-based structures, which provide greater control over the spatial distribution of the enhanced electromagnetic field. Unlike self-assembled colloidal systems, these configurations allow the dimensions, periodicity, and spatial arrangement of the mask features to be predefined, improving geometrical control and potentially enhancing pattern reproducibility. An additional advantage is the possibility of reusing suitably designed masks over multiple irradiation cycles, provided that their optical and mechanical properties remain stable under the applied laser conditions. This can reduce the need for repeated mask fabrication and consequently lower processing costs and material consumption. However, mask-based approaches remain constrained by their predefined geometries, since the production of different patterns generally requires the preparation of new masks. Furthermore, the mask–substrate separation represents an important processing parameter because variations in this distance can modify the intensity and spatial distribution of the enhanced electromagnetic field, ultimately affecting feature dimensions and morphology.

More recently, the use of individually positioned or optically trapped microspheres has expanded the possibilities for localized and geometrically flexible nanofabrication. By controlling the position of individual particles and their irradiation conditions, this approach offers the possibility of producing structures with tailored dimensions and spatial arrangements that are difficult to achieve using conventional self-assembled colloidal monolayers. Nevertheless, the achievable resolution depends on several coupled parameters, including particle diameter, refractive index, positioning accuracy, laser wavelength, pulse characteristics, and the optical and thermal response of the target material. Despite its geometrical flexibility, the sequential manipulation and positioning of individual microspheres generally limit parallel processing and large-area fabrication. In addition, the requirement for specialized optical trapping systems increases experimental complexity and may reduce processing stability. Therefore, the choice of processing strategy involves a trade-off between feature resolution, throughput, pattern flexibility, and experimental complexity, with each approach offering advantages for specific nanofabrication applications. A comparative assessment table (Table 2) of the reported approaches reveals that near-field-enhanced laser processing offers different advantages depending on the optical configuration, particle arrangement, laser parameters, and material properties.

Process control and reproducibility in near-field-assisted laser nanofabrication depend on the stability of both the laser irradiation conditions and the optical configuration used to generate the localized electromagnetic-field enhancement. In particular, pulse-to-pulse fluctuations in laser energy can produce variations in the energy deposited within the substrate, leading to differences in the dimensions, depth, and morphology of the fabricated features. This effect becomes particularly relevant when processing near the ablation threshold, where relatively small variations in incident fluence may result in significant changes in material removal. Such a limitation is relevant to both air and liquid environments, although liquid-assisted processing may introduce additional variations associated with the local refractive index, particle distribution, and liquid-mediated effects. Therefore, reproducible fabrication using colloidal arrangements requires not only stable laser irradiation but also careful control of particle assembly and spatial uniformity. Similar considerations

apply to photoresist-based optical masks. Although their predefined geometries provide improved control over the spatial distribution of the enhanced electromagnetic fields, pulse-to-pulse laser energy fluctuations may still result in variations in material removal and, consequently, in the dimensions and morphology of the fabricated features. Furthermore, variations in mask–substrate separation can modify the local field enhancement, introducing additional sources of dimensional variability. Thus, the reproducibility of mask-assisted processing depends on maintaining both stable irradiation conditions and a well-defined mask–substrate configuration.

Table 2. The main advantages and limitations of the near-field laser processing methods discussed in this review.

Processing Method	Particle Size	Fabricated Feature Size (Material)	Throughput	Arbitrary Processing Configuration	Main Advantages	Practical Limitations
Colloidal lithography assisted laser processing in air and liquids [49,50,52,70,71]	390 nm; 700 nm (SiO_2) [49]	200 nm; 300 nm (Si)	relatively high	No. Usually limited to holes in hexagonal configuration given by the auto arranged effect.	- parallel large-area processing - periodic patterns; - tunable feature dimensions - liquid refractive index provides an additional optical-control parameter	- self-assembly defects, - particle aggregation, - nonuniform coverage; - limited pattern flexibility; - sensitivity to particle–substrate spacing; - possible thermal damage, cracks; - liquid-related instability
	1 µm (polystyrene) [50]	153–191 nm (PMMA; TOPAS)				
	5 µm (SiO_2) [52]	354 nm (Si)				
	700 nm; 3 µm (SiO_2) [71]	300 nm; 400 nm–1.3 µm (Si)				
	8 µm (SiO_2) [70]	Below 600 nm (Si)				
Trapped Microsphere-assisted processing in air [55]	50 µm (dielectric) [55]	50 nm–60 nm (Sb_2S_3 thin films)	relatively low	YES. Microspheres positioned on or near the substrate and irradiated under ambient conditions	- no liquid handling; - relatively simple configuration; - potential for very small features	- material-specific response; - sensitivity to microsphere positioning; - thermal effects
Lithographically patterned optical/photoresist masks [56,57]	1 µm (PMMA) [56,57]	250 nm–800 nm (Si, As_2S_3)	potentially high	YES. Predefined photoresist mask positioned above the substrate;	- single femtosecond laser pulse; - reproducible pattern design; - parallel fabrication; - optical mask reutilization	- requires mask fabrication and alignment; - sensitivity to mask–substrate spacing and laser fluence

In contrast, optically trapped or individually positioned microspheres provide improved control over particle positioning, reducing the uncertainties associated with spontaneous particle self-assembly. This approach can therefore offer better control over the spatial location and geometrical consistency of the fabricated features. However, the individual manipulation and positioning of microspheres are time-consuming, limiting processing throughput and large-area fabrication. Furthermore, maintaining a stable relative position between the microsphere and the substrate during irradiation is essential. Even small fluctuations in particle position or particle–substrate separation can modify the local electromagnetic-field distribution, resulting in variations in the dimensions and morphology of the imprinted structures.

From a scalability perspective, particle-lens arrays and colloidal monolayers provide promising platforms for increasing fabrication throughput, whereas individual microspheres offer greater flexibility for localized processing. However, extending these approaches towards reproducible large-area manufacturing requires improved control over particle arrangement, optical alignment, and irradiation uniformity. No single configuration simultaneously maximizes resolution, throughput, pattern flexibility, and reproducibility.

Future developments should therefore focus on combining controlled particle arrangements with tunable optical-field distributions and optimized irradiation conditions to improve the reliability and scalability of near-field laser processing.

5. Emerging Trends

Recent developments in near-field laser materials processing indicate a shift from conventional particle-assisted configurations towards more flexible and controllable optical processing strategies. Building on the field-enhancement mechanisms and processing approaches discussed above, current research directions include the development of engineered particle arrangements, improved control over the spatial distribution of localized electromagnetic fields, and the integration of optical and chemical effects in liquid-assisted processing [63,68,71–73]. Particular interest is directed towards combining parallel nanofabrication with greater flexibility in pattern geometry, allowing the simultaneous formation of multiple features while maintaining control over their dimensions and spatial distribution [73]. Furthermore, advances in ultrafast laser sources and optical field manipulation offer opportunities to optimize energy deposition and reduce unwanted thermal effects. The integration of in situ monitoring, quantitative surface characterization, and statistical evaluation represents another important direction, particularly for improving process reproducibility and identifying suitable processing conditions [74].

Unlike conventional microsphere-assisted near-field processing, which relies on localized electromagnetic-field enhancement produced by light scattering and photonic nanojet formation, new advances in ultrafast laser processing have opened new perspectives for overcoming the optical diffraction limit and achieving nanoscale precision in direct laser nanofabrication. The development of Optical Focused Ion Beam (O-FIB) by Li et al. [75] and Super-Stealth Dicing (SSD) by Li et al. [76] demonstrates the potential of exploiting localized optical near-field enhancement and self-organized laser–matter interactions for high-resolution material processing. While O-FIB enables sub-20 nm surface nanostructuring under atmospheric conditions, SSD extends these capabilities to the interior of transparent solids, achieving nanometric cutting widths and exceptionally high aspect ratios exceeding 10,000.

5.1. Optical Far-Field-Induced Near-Field Breakdown

Li et al. introduced an innovative optical nanofabrication technique, termed Optical Focused Ion Beam (O-FIB), based on far-field-induced near-field enhancement, enabling direct nanoscale patterning under atmospheric conditions [75]. This approach represents a significant advancement over conventional focused ion beam (FIB) processing by eliminating the need for vacuum environments and avoiding ion implantation while maintaining comparable fabrication resolution. The proposed method employs femtosecond laser pulses to generate initial nanoholes through nonlinear multiphoton absorption. Subsequent laser irradiation induces strong optical near-field enhancement at the nanohole boundaries, resulting in highly localized energy deposition and material ablation beyond the conventional optical diffraction limit. Using an 800 nm femtosecond laser, the authors experimentally demonstrated nanogrooves with widths as small as 18 ± 3 nm, corresponding to approximately $\lambda/40$, Figure 8. Furthermore, the technique provides precise control over nanostructure geometry through dynamic adjustment of laser polarization, enabling the fabrication of complex curved patterns with turning radii down to 100 nm, groove separations of 50 nm, and alignment errors below 10 nm. An important achievement of this work is the identification of a self-regulation mechanism associated with optical near-field confinement, which enables reproducible nanogroove formation despite variations in the initial nanohole dimensions and fluctuations in the laser scanning trajectory. Addition-

ally, the authors demonstrated a large-area printing strategy based on the simultaneous extension of multiple pre-existing nanoholes during scanning, highlighting the potential for parallel processing and improved fabrication throughput. Nevertheless, the experimental validation was primarily performed on titanium oxide thin films, and further investigation is required to establish its applicability across a broader range of materials and its scalability for industrial manufacturing.

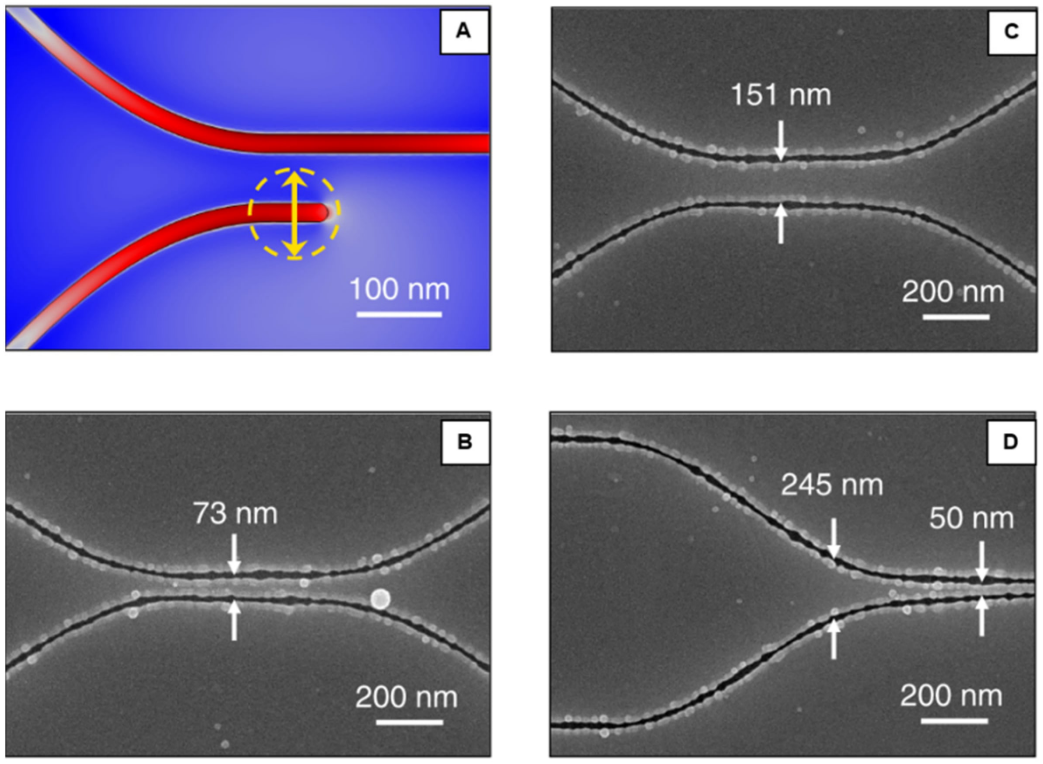


Figure 8. Free writing of arbitrary planar nanogrooves using polarization control. (**A**) polarization perpendicular to the line trajectory; (**B**–**D**) patterns with different separation (reprinted with permission from [75]).

5.2. Near-Field Enhancement Drives a Nanostructure Growth Mechanism

An advanced ultrafast laser nanofabrication technique, termed Super-Stealth Dicing (SSD), capable of producing high-aspect-ratio nanostructures with unprecedented precision inside transparent solid materials was reported by Li et al. [76]. This approach addresses a fundamental limitation of conventional laser machining, namely the trade-off between lateral processing resolution and longitudinal fabrication depth imposed by optical diffraction. By exploiting self-organized laser–matter interactions, SSD enables nanoscale cutting with widths of only a few tens of nanometers while achieving exceptionally high aspect ratios. The underlying mechanism relies on back-scattering interference and near-field enhancement, in which incident femtosecond laser pulses interfere with light back-scattered from laser-induced nanoscale modifications (nano-seeds). This interference promotes the formation of secondary nano-seeds along the laser propagation direction, while localized optical near-field enhancement drives their elongation and interconnection into continuous nano-lines. The resulting positive feedback mechanism enables highly confined and relatively uniform energy deposition over extended depths, overcoming the conventional limitations associated with laser focusing. Using 515 nm femtosecond laser pulses, the authors demonstrated nano-lines with widths as small as 10 nm extending approximately 95 μm in a single scan, corresponding to aspect ratios approaching 10,000. A particularly

significant achievement is the demonstration of nanometric cutting widths down to 7 nm in lithium niobate, together with nanostructures extending to depths of 230 μm with characteristic widths of 15 nm, corresponding to aspect ratios exceeding 15,000. Furthermore, the technique exhibits a self-regulation mechanism that ensures reproducible nanostructure formation, with experimentally demonstrated line widths of 45.8 ± 2.5 nm. The versatility of SSD was validated across several transparent materials, including fused silica, lithium niobate, lithium tantalate, sapphire, YAG crystals, and β-Ga_2O_3. The authors also demonstrated the fabrication of complex micro-optical structures, including nanorods, ultrathin waveplates, and microprisms, with cutting-surface roughness as low as 9.4 nm and optical retardance control with sub-nanometer precision. This work represents a substantial advancement in ultrafast laser nanomachining by combining deep-subwavelength resolution, extremely high aspect ratios, and three-dimensional processing capabilities. Unlike conventional approaches that rely primarily on beam shaping, SSD exploits the intrinsic feedback between optical scattering, near-field enhancement, and material modification to achieve high-precision nano-structuring. Its applicability to various functional crystals and its demonstrated ability to fabricate high-quality optical components highlight its potential for integrated photonics, optoelectronics, semiconductor manufacturing, and advanced micro-optical systems. Nevertheless, practical implementation may require additional processing steps, such as chemical etching or controlled mechanical separation, while manufacturing throughput and industrial scalability remain to be further established.

These developments suggest a promising transition from conventional diffraction-limited laser machining toward near-field-assisted, self-regulated nanofabrication, in which the spatial distribution of deposited energy is governed by dynamic interactions between the incident laser field and laser-induced nanostructures. Future research could focus on integrating these mechanisms with advanced beam shaping, adaptive polarization control, and parallel laser processing to achieve greater flexibility, improved throughput, and reproducible three-dimensional nanofabrication. Furthermore, extending these approaches to a wider range of functional materials and developing precise control over nanoscale energy localization could enable the fabrication of increasingly complex photonic and optoelectronic architectures. Combining the principles demonstrated by O-FIB and SSD may provide a foundation for a new generation of high-resolution, scalable, and potentially industrially applicable laser nanomanufacturing technologies, bridging the gap between nanoscale fabrication precision and practical manufacturing requirements.

6. Conclusions

Near-field laser materials processing represents a promising approach for overcoming the diffraction limit of conventional optical systems, enabling highly localized material modification and the fabrication of nanostructures with dimensions substantially smaller than the irradiation wavelength. A major advantage of near-field laser processing is its capability for parallel nanofabrication, offering the possibility of significantly increasing processing throughput compared with conventional serial laser writing. Self-assembled colloidal arrays enable simultaneous fabrication of periodic nanostructures, while optically trapped microspheres and engineered dielectric masks provide additional control over feature positioning and geometry. Single-pulse processing, relatively simple experimental configurations, and potentially reusable optical masks further support the development of cost-effective and scalable nanomanufacturing strategies. Processing in liquid environments introduces additional control over electromagnetic field localization through changes in the surrounding refractive index, while influencing heat transfer, material removal, and laser-induced chemical reactions. These effects enable different surface morphologies and provide opportunities for more complex structuring using multilayer colloidal assemblies.

Nevertheless, several limitations remain, particularly regarding particle positioning, pattern flexibility, laser irradiation uniformity, and reproducibility. Furthermore, the relationship between electromagnetic field enhancement and the final material morphology is influenced by nonlinear, thermal, and mechanical processes that require further investigation. From an industrial perspective, further improvements are required in process stability, reproducibility, large-area uniformity, processing throughput, and compatibility with different materials and substrates. The development of reliable particle assembly and positioning strategies, optimized irradiation configurations, and robust process-control methods will therefore be essential for translating the demonstrated laboratory approaches into scalable manufacturing technologies. Continued progress in optical-field engineering, process reproducibility, and manufacturing scalability could establish this technique as a versatile platform for high-resolution, high-throughput nanomanufacturing.

Author Contributions: Conceptualization, I.A. and F.J.; writing—original draft preparation, I.A.; writing—review and editing, L.I., F.J. and M.Z. All authors have read and agreed to the published version of the manuscript.

Funding: This work was supported by a grant of the Ministry of Research, Innovation and Digitization, CCCDI-UEFISCDI, project number PN-IV-P7-7.1-PED-2024-2355, within PNCDI IV.

Data Availability Statement: Data will be made available on request.

Acknowledgments: We also acknowledge the support of the National Interest Infrastructure facility, IOSIN–CETAL, INFLPR.

Conflicts of Interest: The authors declare no conflicts of interest.

References

1. Graydon, O. Laser-Printed Microelectronics. *Nat. Photonics* **2023**, *17*, 297. [CrossRef]
2. Jia, Y.; Chen, F. Recent Progress on Femtosecond Laser Micro-/Nano-Fabrication of Functional Photonic Structures in Dielectric Crystals: A Brief Review and Perspective. *APL Photonics* **2023**, *8*, 090901. [CrossRef]
3. Miller, P.R.; Aggarwal, R.; Doraiswamy, A.; Lin, Y.J.; Lee, Y.-S.; Narayan, R.J. Laser Micromachining for Biomedical Applications. *JOM* **2009**, *61*, 35–40. [CrossRef]
4. Lipovka, A.; Garcia, A.; Abyzova, E.; Fatkullin, M.; Song, Z.; Li, Y.; Wang, R.; Rodriguez, R.D.; Sheremet, E. Laser Processing of Emerging Nanomaterials for Optoelectronics and Photocatalysis. *Adv. Opt. Mater.* **2024**, *12*, 2303194. [CrossRef]
5. Yu, K.; Shi, H.; Zhang, P.; Yu, Z.; Yan, H.; Lu, Q. Micro/Nanoengineering of Functionalized Metal Surfaces Based on Short/Ultra-Short-Pulsed Lasers: A Review. *J. Mater. Sci.* **2024**, *59*, 1819–1866. [CrossRef]
6. Beresna, M.; Falak, P.L.; Lee, T.; Holmes, C.; Masoudi, A.; Phillips, D.; Vettenburg, T.; Brambilla, G. Ultrafast Laser Processing for Optical Fibre Sensing. In *Proceedings of the Laser + Photonics for Advanced Manufacturing*; Lecler, S., Pfleging, W., Courvoisier, F., Eds.; SPIE: Strasbourg, France, 2024; p. 49.
7. He, M.; Hou, Y.; Li, G.; Mu, W.; Wu, Y.; Liu, M. Laser Micro/Nanofabrication of Superhydrophobic Surfaces: Fundamentals, Processing Strategies, and Applications. *Coatings* **2026**, *16*, 788. [CrossRef]
8. Pohl, D.W. Optics at the Nanometre Scale. *Philos. Trans. R. Soc. London. Ser. A Math. Phys. Eng. Sci.* **2004**, *362*, 701–717. [CrossRef] [PubMed]
9. Guan, L.; Cao, C.; Liu, X.; Liu, Q.; Qiu, Y.; Wang, X.; Yang, Z.; Lai, H.; Sun, Q.; Ding, C.; et al. Light and Matter Co-Confined Multi-Photon Lithography. *Nat. Commun.* **2024**, *15*, 2387. [CrossRef] [PubMed]
10. Tojar, G.; Saha, S.K. Suppressing Proximity Effects during Rapid Serial Two-Photon Lithography through Tuning of Reaction–Diffusion Kinetics. *J. Appl. Phys.* **2026**, *139*, 024901. [CrossRef]
11. Cao, C.; Xia, X.; Shen, X.; Wang, X.; Yang, Z.; Liu, Q.; Ding, C.; Zhu, D.; Kuang, C.; Liu, X. Ultra-High Precision Nano Additive Manufacturing of Metal Oxide Semiconductors via Multi-Photon Lithography. *Nat. Commun.* **2024**, *15*, 9216. [CrossRef] [PubMed]
12. Hambitzer, L.; Hornbostel, J.M.; Roolfs, L.; Prediger, R.; Kluck, S.; Zheng, K.; Lee-Thedieck, C.; Kotz-Helmer, F. Bioactive Glass Microscaffolds Fabricated by Two-Photon Lithography. *Adv. Mater.* **2025**, *37*, 2504475. [CrossRef] [PubMed]
13. Buzio, M.; Gini, M.; Schneider, T.C.; Stajkovic, N.; Ingebrandt, S.; De Laporte, L.; Offenhäusser, A.; Criscuolo, V.; Santoro, F. 3D Micropatterning of PEDOT:PSS/Gelatin Conductive Hydrogels via Two-Photon Lithography for Soft Bioelectronics. *npj Flex. Electron.* **2026**, *10*, 19. [CrossRef]

14. Cao, C.; Fang, J.; Li, X.; Zhang, A.; Shen, X.; Ci, J.; Zhao, X.; Kuang, C. RAFT Polymerization Assisted Multi-Photon Lithography Enables High-Precision and Living 3D Printing. *Addit. Manuf.* **2026**, *121*, 105178. [CrossRef]
15. Zhang, A.; Lai, H.; Cao, C.; Shen, X.; Zhang, J.; Liu, Q.; Tong, D.; Kuang, C.; Liu, X. In-Situ Two-Photon Induced Chemical Bonding Enables Initiator-Free Nanofabrication of Biocompatible Microstructure. *Opt. Laser Technol.* **2026**, *193*, 114344. [CrossRef]
16. Cao, C.; Zhang, A.; Li, X.; Fang, J.; Shen, X.; Ci, J.; Kuang, C. Thiol-Ene Click Two-Photon Polymerization Photoresists towards Optical Nanoprinting. *Opt. Laser Technol.* **2026**, *203*, 115525. [CrossRef]
17. Kim, H.; Saha, S.K. Grayscale Projection Two-Photon Lithography Using Sub-Diffraction Motifs for Ultrafast and Precise Nanoscale 3D Printing. *Nat. Commun.* **2026**, *17*, 6981. [CrossRef] [PubMed]
18. Yu, Y.; Zhu, Z.; Willenberg, B.; Pupeikis, J.; Phillips, C.R.; Chen, S.-C. Closed-Loop High-Precision Two-Photon Lithography Based on a Multiplexed Single-Cavity Dual-Comb Laser. *Nat. Commun.* **2026**, *17*, 7135. [CrossRef] [PubMed]
19. Luk'yanchuk, B.S.; Paniagua-Domínguez, R.; Minin, I.; Minin, O.; Wang, Z. Refractive Index Less than Two: Photonic Nanojets Yesterday, Today and Tomorrow [Invited]. *Opt. Mater. Express* **2017**, *7*, 1820. [CrossRef]
20. Chen, Y.-J.; Hsu, J.-H.; Lin, H.-N. Fabrication of Metal Nanowires by Atomic Force Microscopy Nanoscratching and Lift-off Process. *Nanotechnology* **2005**, *16*, 1112–1115. [CrossRef]
21. Case, M.A.; McLendon, G.L.; Hu, Y.; Vanderlick, T.K.; Scoles, G. Using Nanografting to Achieve Directed Assembly of de Novo Designed Metalloproteins on Gold. *Nano Lett.* **2003**, *3*, 425–429. [CrossRef]
22. Münzer, H.-J.; Mosbacher, M.; Bertsch, M.; Zimmermann, J.; Leiderer, P.; Boneberg, J. Local Field Enhancement Effects for Nanostructuring of Surfaces. *J. Microsc.* **2001**, *202*, 129–135. [CrossRef] [PubMed]
23. Mie, G. Beiträge Zur Optik Trüber Medien, Speziell Kolloidaler Metallösungen. *Ann. Der Phys.* **1908**, *330*, 377–445. [CrossRef]
24. Tzarouchis, D.; Sihvola, A. Light Scattering by a Dielectric Sphere: Perspectives on the Mie Resonances. *Appl. Sci.* **2018**, *8*, 184. [CrossRef]
25. Luk'yanchuk, B.S. (Ed.) *Laser Cleaning: Optical Physics, Applied Physics, and Materials Science*; World Scientific: River Edge, NJ, USA, 2002.
26. Dorodnyy, A.; Smajic, J.; Leuthold, J. Mie Scattering for Photonic Devices. *Laser Photonics Rev.* **2023**, *17*, 2300055. [CrossRef]
27. Gouesbet, G.; Gréhan, G. *Generalized Lorenz-Mie Theories*; Springer: Berlin/Heidelberg, Germany, 2011.
28. Darafsheh, A. Photonic Nanojets and Their Applications. *J. Phys. Photonics* **2021**, *3*, 022001. [CrossRef]
29. Mundy, W.C.; Roux, J.A.; Smith, A.M. Mie Scattering by Spheres in an Absorbing Medium. *J. Opt. Soc. Am.* **1974**, *64*, 1593. [CrossRef]
30. Bohren, C.F.; Gilra, D.P. Extinction by a Spherical Particle in an Absorbing Medium. *J. Colloid Interface Sci.* **1979**, *72*, 215–221. [CrossRef]
31. Liou, K.-N. A Complementary Theory of Light Scattering by Homogeneous Spheres. *Appl. Math. Comput.* **1977**, *3*, 331–358. [CrossRef]
32. Lecler, S.; Perrin, S.; Leong-Hoi, A.; Montgomery, P. Photonic Jet Lens. *Sci. Rep.* **2019**, *9*, 4725. [CrossRef] [PubMed]
33. Yee, K. Numerical Solution of Initial Boundary Value Problems Involving Maxwell's Equations in Isotropic Media. *IEEE Trans. Antennas Propag.* **1966**, *14*, 302–307. [CrossRef]
34. Ionel, L.E. Numerical Analysis of Non-Collinear Coherently Combined Laser Beams Interaction with Micro-Structured Targets. *Opt. Commun.* **2021**, *498*, 127234. [CrossRef]
35. Ionel, L.; Viespe, C. Numerical Investigation of Enhanced High-Intensity Laser–Matter Interactions in Nanowire-Coated Conical Targets. *Nanomaterials* **2025**, *15*, 1763. [CrossRef] [PubMed]
36. Ionel, L. Characterising Spatio-Temporal Coupling of Tightly Focused Femtosecond Laser Pulses in Micro-Structured Dispersive Materials. *Photonics* **2024**, *11*, 689. [CrossRef]
37. Anghel, I. Numerical Investigation of Photonic Crystals Structure on Zinc Oxide Film. *Optik* **2019**, *185*, 282–286. [CrossRef]
38. Anghel, I.; Petris, A. Design of an All-Optical Tunable 2D Photonic Crystal in As2S3 Film. *Opt. Commun.* **2025**, *574*, 131247. [CrossRef]
39. Anghel, I.; Jipa, F.; Andrei, A.; Simion, S.; Dabu, R.; Rizea, A.; Zamfirescu, M. Femtosecond Laser Ablation of TiO2 Films for Two-Dimensional Photonic Crystals. *Opt. Laser Technol.* **2013**, *52*, 65–69. [CrossRef]
40. Ulmeanu, M.; Jipa, F.; Luculescu, C.; Moldovan, A.; Zamfirescu, M. Single Pulse near Field Study on a Co(3 Nm)/Cu(6 Nm)/Co(20 Nm) Multilayer Structure by Using a Femtosecond Laser. *Appl. Phys. A* **2011**, *104*, 839–843. [CrossRef]
41. Chatzizyrli, E.; Rittmeier, A.; Böse, S.; Neumann, J.; Kracht, D.; Hinkelmann, M. Wave Optics Simulation of Surface Roughness for Integrated Photonics Fabricated through Multiphoton Lithography. In *Proceedings of the Integrated Optics: Devices, Materials, and Technologies XXIX*; García-Blanco, S.M., Cheben, P., Eds.; SPIE: San Francisco, CA, USA, 2025; p. 87.
42. Oskooi, A.F.; Roundy, D.; Ibanescu, M.; Bermel, P.; Joannopoulos, J.D.; Johnson, S.G. Meep: A Flexible Free-Software Package for Electromagnetic Simulations by the FDTD Method. *Comput. Phys. Commun.* **2010**, *181*, 687–702. [CrossRef]
43. Sulemani, M.F. Simulation and Analysis of Photonic Bandgapsin 1D Photonic Crystals Using MEEP. *Int. J. Phys. Res. Appl.* **2024**, *7*, 127–131. [CrossRef]

44. Atanasov, P.A.; Nedyalkov, N.N.; Fukata, N.; Jevasuwan, W. Ag and Au Nanostructures for Surface-enhanced Raman Spectroscopy of Mospilan 20 SP (Acetamiprid). *J. Raman Spectrosc.* **2020**, *51*, 2398–2407. [CrossRef]
45. Lv, Z.; Zhang, Y.; Peng, X.; Wu, C.; Zhang, Y.; Ke, Z.; Peng, Y.; Chen, J.; Yu, Z.; Han, L.; et al. Near-Field Scanning of Microfiber Evanescent Fields Using a Tapered Nanofiber Probe. *Opt. Laser Technol.* **2026**, *198*, 114947. [CrossRef]
46. Avramov-Zamurovic, S.; Sivaprakasam, V.; Hart, M.B.; McCarthy, J.E. Laser Beam Carrying Orbital Angular Momentum Scattering from a Particle: Near-Field Intensity and Phase Numerical Study. *J. Quant. Spectrosc. Radiat. Transf.* **2024**, *329*, 109192. [CrossRef]
47. Ulmeanu, M.; Zamfirescu, M.; Medianu, R. Self-Assembly of Colloidal Particles on Different Surfaces. *Colloids Surf. A Physicochem. Eng. Asp.* **2009**, *338*, 87–92. [CrossRef]
48. Ulmeanu, M.; Anghel, I.; Filipescu, M.; Luculescu, C.; Enculescu, M.; Zamfirescu, M. Periodic Arrays of Nanostructures in Silicon and Gallium Arsenide by Near-Field Enhanced Laser Irradiation in Liquid Precursors. *Colloids Surf. A Physicochem. Eng. Asp.* **2013**, *418*, 47–51. [CrossRef]
49. Ulmeanu, M.; Anghel, I.; Jipa, F.; Filipescu, M.; Enculescu, M.; Zamfirescu, M. Silicon Bump Arrays by Near-Field Enhanced Femtosecond Laser Irradiation in Fluorine Liquid Precursors. *Appl. Surf. Sci.* **2013**, *278*, 301–304. [CrossRef]
50. Afanasiev, A.; Pikulin, A.; Ilyakov, I.; Shishkin, B.; Bityurin, N. Edge Effect at the Microsphere Colloidal Array in Near-Field Particle Lithography on Polymer Surfaces. *Surf. Interfaces* **2022**, *29*, 101735. [CrossRef]
51. Hong, M. From Transparent Particle Light Enhancement to Laser Nanoimprinting. *JLMN* **2006**, *1*, 61–66. [CrossRef]
52. Pena, A.; Wang, Z.; Whitehead, D.; Li, L. Direct Writing of Micro/Nano-Scale Patterns by Means of Particle Lens Arrays Scanned by a Focused Diode Pumped Nd:YVO4 Laser. *Appl. Phys. A* **2010**, *101*, 287–295. [CrossRef]
53. Khanh, N.N.; Yoon, K.B. Facile Organization of Colloidal Particles into Large, Perfect One- and Two-Dimensional Arrays by Dry Manual Assembly on Patterned Substrates. *J. Am. Chem. Soc.* **2009**, *131*, 14228–14230. [CrossRef] [PubMed]
54. Cai, W.; Piestun, R. Patterning of Silica Microsphere Monolayers with Focused Femtosecond Laser Pulses. *Appl. Phys. Lett.* **2006**, *88*, 111112. [CrossRef]
55. Yin, J.; Luo, H.; Cao, T.; Hong, M. Polarization-Independent Surface Nanostructuring by Femtosecond Laser Irradiation via Microsphere in Far Field and Ambient Air. *Light. Sci. Appl.* **2026**, *15*, 114. [CrossRef] [PubMed]
56. Jipa, F.; Dinescu, A.; Filipescu, M.; Anghel, I.; Zamfirescu, M.; Dabu, R. Laser Parallel Nanofabrication by Single Femtosecond Pulse Near-Field Ablation Using Photoresist Masks. *Opt. Express* **2014**, *22*, 3356. [CrossRef] [PubMed]
57. Jipa, F.; Velea, A.; Luculescu, C.; Zamfirescu, M. Sub-Wavelength Parallel Patterning of As_2S_3 Photosensitive Glass by Single-Pulse Femtosecond Laser near-Field Enhancement. *Surf. Interfaces* **2026**, *98*, 110341. [CrossRef]
58. Khudiyev, T.; Huseyinoglu, E.; Bayindir, M. Non-Resonant Mie Scattering: Emergent Optical Properties of Core-Shell Polymer Nanowires. *Sci. Rep.* **2014**, *4*, 4607. [CrossRef] [PubMed]
59. Linz, N.; Freidank, S.; Liang, X.-X.; Vogel, A. Laser-Induced Plasma Formation and Cavitation in Water: From Nanoeffects to Extreme States of Matter. *Rep. Prog. Phys.* **2025**, *88*, 088501. [CrossRef] [PubMed]
60. Kaneko, R.; Ichikawa, H.; Hosaka, M.; Sone, Y.; Imura, Y.; Wang, K.-H.; Kawai, T. Hole, Convex, and Silver Nanoparticle Patterning on Polystyrene Nanosheets by Colloidal Photolithography at Air–Water Interfaces. *Langmuir* **2022**, *38*, 8153–8159. [CrossRef] [PubMed]
61. Boneberg, J.; Leiderer, P. Optical Near-Field Imaging and Nanostructuring by Means of Laser Ablation. *Opto-Electron. Sci.* **2022**, *1*, 210003. [CrossRef]
62. Lai, S.; Liu, Y.; Gong, L.; Zhao, Y.; Zhang, C.; Han, B. Laser-Induced Surface Structures at Polymer Surfaces Irradiated by Ns-UV-Laser in Water Confinement and in Air. *Opt. Laser Technol.* **2024**, *168*, 109871. [CrossRef]
63. Ulmeanu, M.; Jipa, F.; Radu, C.; Enculescu, M.; Zamfirescu, M. Large Scale Microstructuring on Silicon Surface in Air and Liquid by Femtosecond Laser Pulses. *Appl. Surf. Sci.* **2012**, *258*, 9314–9317. [CrossRef]
64. Tao, Y.; Wang, Z.; Hu, S.; Feng, Y.; Yang, F.; Li, G. Improving the Quality of Laser Drilling by Assisted Process Methods of Static Solution and Mist Blowing. *Micromachines* **2024**, *15*, 515. [CrossRef] [PubMed]
65. Tam, A.C.; Park, H.K.; Grigoropoulos, C.P. Laser Cleaning of Surface Contaminants. *Appl. Surf. Sci.* **1998**, *127–129*, 721–725. [CrossRef]
66. Krivonosov, A.; Zuev, D.; Kaputkina, S.; Mikhailovskii, V.; Egorova, E.; Ageev, E.; Odintsova, G. Evolution of Size Distribution of Si Nanoparticles Produced by Pulsed Laser Ablation in Water. *Opt. Quantum Electron.* **2020**, *52*, 158. [CrossRef]
67. Zhang, H.; Li, X.; Peng, Y.; Wang, K.; Wang, D. Liquid-Confined Femtosecond Laser Fabrication of High-Aspect-Ratio Microchannels for Efficient Thermal Management. *J. Manuf. Process.* **2026**, *157*, 1001–1014. [CrossRef]
68. Ulmeanu, M.; Petkov, P.; Ursescu, D.; Maraloiu, V.A.; Jipa, F.; Brousseau, E.; Ashfold, M.N.R. Pattern Formation on Silicon by Laser-Initiated Liquid-Assisted Colloidal Lithography. *Nanotechnology* **2015**, *26*, 455303. [CrossRef] [PubMed]
69. Wang, Z.B.; Guo, W.; Pena, A.; Whitehead, D.J.; Luk'yanchuk, B.S.; Li, L.; Liu, Z.; Zhou, Y.; Hong, M.H. Laser Micro/Nano Fabrication in Glass with Tunable-Focus Particle Lens Array. *Opt. Express* **2008**, *16*, 19706. [CrossRef] [PubMed]
70. Rahman, R.A.; Uenohara, T.; Mizutani, Y.; Takaya, Y. Second Harmonic Generation-Enhanced Photonic Nanojet Machining in Water Medium with Position Control for Submicrometer Ablation. *Nanomanuf Metrol.* **2025**, *8*, 32. [CrossRef]

71. Ulmeanu, M.; Grubb, M.P.; Jipa, F.; Quignon, B.; Ashfold, M.N.R. 3-D Patterning of Silicon by Laser-Initiated, Liquid-Assisted Colloidal (LILAC) Lithography. *J. Colloid Interface Sci.* **2015**, *447*, 258–262. [CrossRef] [PubMed]
72. Guo, W.; Wang, Z.B.; Li, L.; Liu, Z.; Luk'yanchuk, B.; Whitehead, D.J. Chemical-Assisted Laser Parallel Nanostructuring of Silicon in Optical near Fields. *Nanotechnology* **2008**, *19*, 455302. [CrossRef] [PubMed]
73. Surdo, S.; Duocastella, M.; Diaspro, A. Nanopatterning with Photonic Nanojets: Review and Perspectives in Biomedical Research. *Micromachines* **2021**, *12*, 256. [CrossRef] [PubMed]
74. Yildirim, K.; Nagarajan, B.; Tjahjowidodo, T.; Castagne, S. Review of In-Situ Process Monitoring for Ultra-Short Pulse Laser Micromanufacturing. *J. Manuf. Process.* **2025**, *133*, 1126–1159. [CrossRef]
75. Li, Z.-Z.; Wang, L.; Fan, H.; Yu, Y.-H.; Chen, Q.-D.; Juodkazis, S.; Sun, H.-B. O-FIB: Far-Field-Induced near-Field Breakdown for Direct Nanowriting in an Atmospheric Environment. *Light. Sci. Appl.* **2020**, *9*, 41. [CrossRef] [PubMed]
76. Li, Z.-Z.; Fan, H.; Wang, L.; Zhang, X.; Zhao, X.-J.; Yu, Y.-H.; Xu, Y.-S.; Wang, Y.; Wang, X.-J.; Juodkazis, S.; et al. Super-Stealth Dicing of Transparent Solids with Nanometric Precision. *Nat. Photonics* **2024**, *18*, 799–808. [CrossRef]

Disclaimer/Publisher's Note: The statements, opinions and data contained in all publications are solely those of the individual author(s) and contributor(s) and not of MDPI and/or the editor(s). MDPI and/or the editor(s) disclaim responsibility for any injury to people or property resulting from any ideas, methods, instructions or products referred to in the content.